Supporting Information

1. Poroelastic Model for Estimating the Collagen Matrix Mechanical and Transport Properties

The poroelastic model used in this study is based on Armstrong et al. [1] which previously developed analytical solutions for deformation, pressure and stress during unconfined compression of a poroelastic specimen. In the subsequent subsections, we provide a brief outline of the model definitions, assumptions and derivation.

1.1. Model Definitions

We consider unconfined compression of a cylindrical specimen of radius a between two parallel plates as shown in Figure S1. The loading program represents application of an either compressive force or strain profile through a moveable clamp. The specimen is assumed to be porous with a solid matrix exhibiting linear elastic behavior. The pores of the specimen are saturated with an incompressible fluid that is pressurized and gets gradually discharged through the unconfined lateral surfaces of the specimen in response to the applied compressive loading.

Important definitions that are used in the derivation are provided in Table S1.

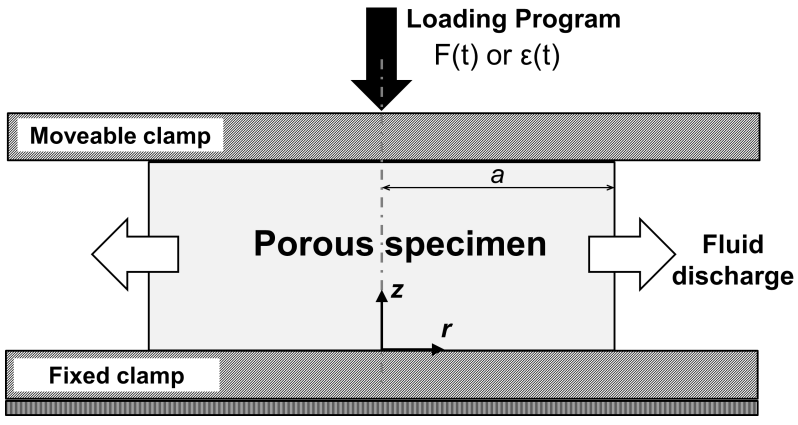

Figure S1. Unconfined compression of porous specimen saturated with fluid. Problem setup.

Table S1. Poroelastic Model Definitions.

Definition	Symbol	Unit
Radius of specimen	a	m
Elastic modulus (solid matrix)	E_s	Pa
Shear modulus (Lame's second parameter)	μ_s	Pa
Compressibility modulus (Lame's first parameter)	λ_s	Pa
Aggregate modulus	$H_a = \lambda_s + 2\mu_s$	Pa
Poisson's Ratio (Solid matrix)	ν_s	1
Hydraulic conductivity	K	m^2/Pa.s
Prescribed strain history	$\varepsilon(t)$	1
Prescribed load history	$F(t)$	N
Nondimensional quantities	(^)	-
Laplace transform quantities	(-)	-
Porosity	ϕ_f	1
Interstitial pressure	p	Pa
Stress tensor	$\boldsymbol{\sigma}$	Pa
Fluid and solid velocities	$\dot{\vec{v}}_f, \dot{\vec{v}}_s$	m/s
Displacement vector	$\vec{u} = (u_r, u_\theta, u_z) = (u, u_\theta, w$	m

1.2. Assumptions

i. Axisymmetric geometry, displacement and pressure fields.

$$u_\theta = 0, \ \frac{\partial(.)}{\partial\theta} = 0 \tag{1}$$

ii. Compressive strain in the axial direction is homogeneous. This is true if the parallel plates are impervious and frictionless.

$$u_z = w(z,t) = z \cdot \varepsilon(t) \tag{2}$$

iii. Solid and fluid phases are incompressible. This enables cancellation of densities from equation (5).

iv. Linear elastic solid phase. Enables writing of equation (4).

1.3. Governing Equations

1.3.1 Stress equilibrium

$$\nabla \cdot \boldsymbol{\sigma} = \vec{0} \tag{3}$$

where

$$\boldsymbol{\sigma} = -\frac{p}{\phi_f}\mathbf{I} + \lambda_s e\mathbf{I} + 2\mu_s \boldsymbol{\varepsilon} \tag{4}$$

1.3.2 Mixture mass conservation

$$\nabla \cdot \left(v_f + \frac{\partial \vec{u}}{\partial t} \right) = 0 \tag{5}$$

1.3.3 Conservation of momentum in fluid phase (Darcy's Law)

$$\phi_f \left(\vec{v}_f - \frac{\partial \vec{u}}{\partial t} \right) = -K \nabla p \tag{6}$$

where hydraulic conductivity, K is related to permeability, k, with:

$$K = \frac{k}{\mu} \tag{7}$$

where μ is the dynamic viscosity of the interstitial fluid. Due to assumption (ii), there is no relative fluid velocity in z-directions i.e. $v_{f,z} = v_{s,z} = \partial w / \partial t$, the continuity equation can be integrated in r to obtain fluid velocity in r-direction as:

$$v_{f,r} = -\frac{(1-\phi_f)}{\phi_f}\frac{\partial u}{\partial t} - \frac{r}{2\phi_f}\frac{\partial \varepsilon}{\partial t} \tag{8}$$

Next, equation (4) is substituted in equation (3). Then the pressure is eliminated in equation (3) by using (6). Finally, the radial component equation (3) is simplified by substituting equation (8). The result is:

$$\frac{\partial^2 u}{\partial r^2}+\frac{1}{r}\frac{\partial u}{\partial r}-\frac{y}{r^2}=\frac{1}{H_A K_{hyd}}\frac{\partial u}{\partial t}+\frac{1}{H_A K_{hyd}}\frac{r}{2}\frac{\partial \varepsilon}{\partial t} \tag{9}$$

Initially, the specimen is undeformed, the flow field is stagnant and the boundary conditions at free lateral interface ($r=a$) are $\sigma_{rr}=0,\ \ p=0$.

1.4. Nondimensionalization

$$\hat{r}= \qquad \hat{u}= \qquad \hat{p}= \qquad \hat{\sigma}_{ij}= \qquad \hat{F}=\frac{F}{\mu_s \pi} \qquad \hat{t}=$$

where nondimensional variables are denoted by "^". $t_g=\frac{H_A K_{hyd}}{a^2}$ is the diffusion time scale for interstitial fluid transport. t_g is also called the "gel diffusion time".

1.5. Laplace Transform

Considering Laplace transformation of equation (9) in nondimensional time domain, we obtain:

$$\frac{\partial^2 \bar{u}}{\partial \hat{r}^2}+\frac{1}{\hat{r}}\frac{\partial \bar{u}}{\partial \hat{r}}-\frac{\bar{u}}{\hat{r}^2}-s\bar{u}=\frac{s\bar{\varepsilon}\hat{r}}{2} \tag{10}$$

The solution is to equation (10) is:

$$\bar{u}(\hat{r},s)=-\frac{\bar{\varepsilon}(s)\hat{r}}{2}\frac{I_o\left(\sqrt{s}\right)-\frac{2\mu_s}{H_A}\left[\frac{I_1\left(\sqrt{s}\hat{r}\right)}{\sqrt{s}\hat{r}}+\frac{I_1\left(\sqrt{s}\right)}{\sqrt{s}}\right]}{I_o\left(\sqrt{s}\right)-\frac{2\mu_s}{H_A}\frac{I_1\left(\sqrt{s}\right)}{\sqrt{s}}} \tag{11}$$

where I_0 and I_1 are modified Bessel functions.

1.6. Relationship between Force and Strain

59 By integrating σ_{zz} across the top surface, a relationship between apparent force and strain is obtained:

60
$$\bar{F}(s) = \bar{\varepsilon}(s) \frac{3I_o\left(\sqrt{s}\right) - \frac{8\mu_s}{H_A}\frac{I_1\left(\sqrt{s}\right)}{\sqrt{s}}}{I_o\left(\sqrt{s}\right) - \frac{2\mu_s}{H_A}\frac{I_1\left(\sqrt{s}\right)}{\sqrt{s}}} \tag{12}$$

61 Equation (12) is used to predict the stress-strain curves that arise during the loading program prescribed in
62 dynamic mechanical analysis experiments. The relationships in time domain are obtained by numerical inverse
63 Laplace transform.

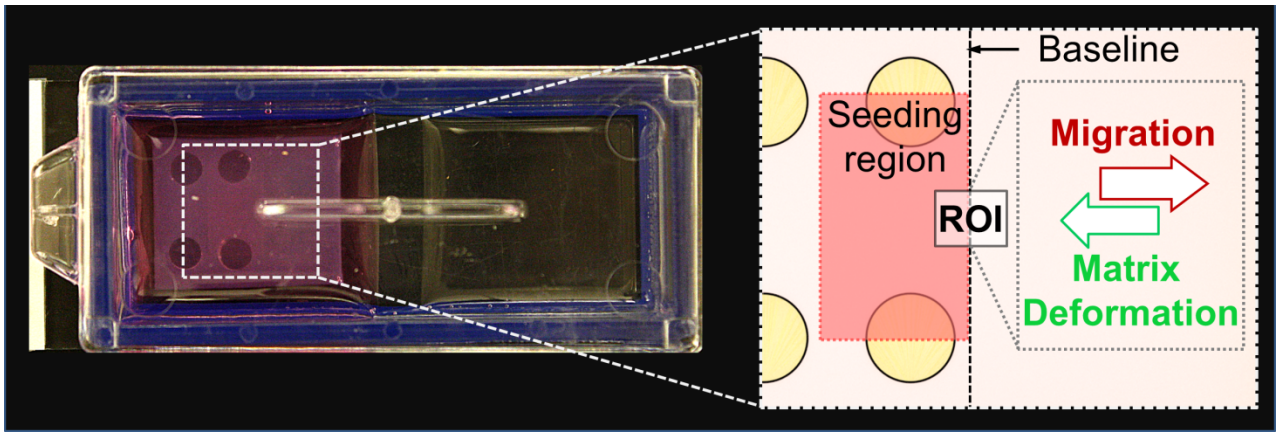

Figure 2. Illustration of the position of the region of interest (ROI) for measurement of cell migration and matrix translocation with respect to culture chamber.

2. Tissue Image Deformetry Based on Incremental Particle Image Velocimetry (I-PIV)

PIV utilizes cross-correlation of a pair of images acquired at successive time points to estimate the instantaneous velocity field. The velocity field was spatially resolved by division of images into multiple overlapping interrogation windows. Interrogation window size was iteratively decreased from 256 x 256 to 64 x 64 pixels with 3 to 4 iterations performed at each window size. The overlap between interrogation windows was set to 50% for all window sizes. The PIV procedure resulted in velocity measurements across 15 min time intervals and over a regular grid of image points with 60 μm spacing. The PIV velocity field was then integrated over time to determine the trajectories of material points representing the translocation of the hydrogel The trajectories calculated by this incremental-PIV (I-PIV) technique were validated against tracer trajectories directly determined by single particle tracking (SPT). Marker displacements velocity magnitudes obtained by I-PIV and SPT were in good agreement (**Figure S2 (b) and (c)**).

Movie S1: Trajectories of cells migrating on low density (1.5 mg/mL) and high density (6.0 mg/mL) collagen matrices determined by time-lapse imaging followed by single particle tracking. Trajectories are superimposed on bright field (left) and quantum dot intensity (right) micrographs.

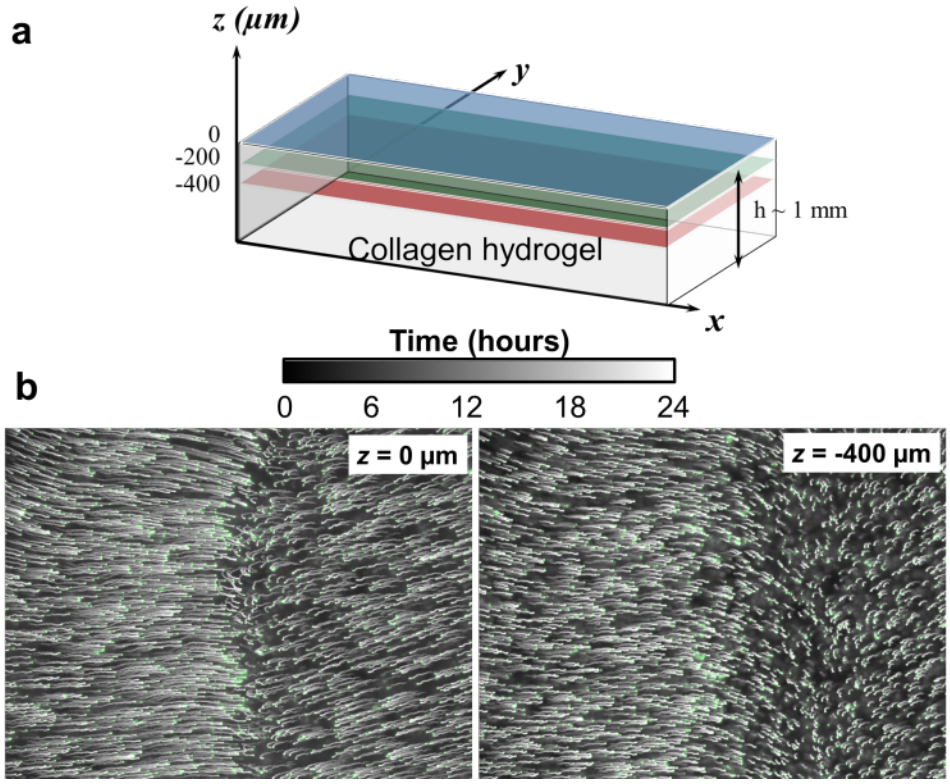

Figure S2. Multi-plane imaging of fluorescent tracers within collagen matrix. (a) Images were acquired across collagen hydrogel at multiple focal planes. (b) Time-coded fluorescence images showing trajectories of matrix tracers at the surface of (z = 0 μm) and within (z = -400 μm) the collagen.

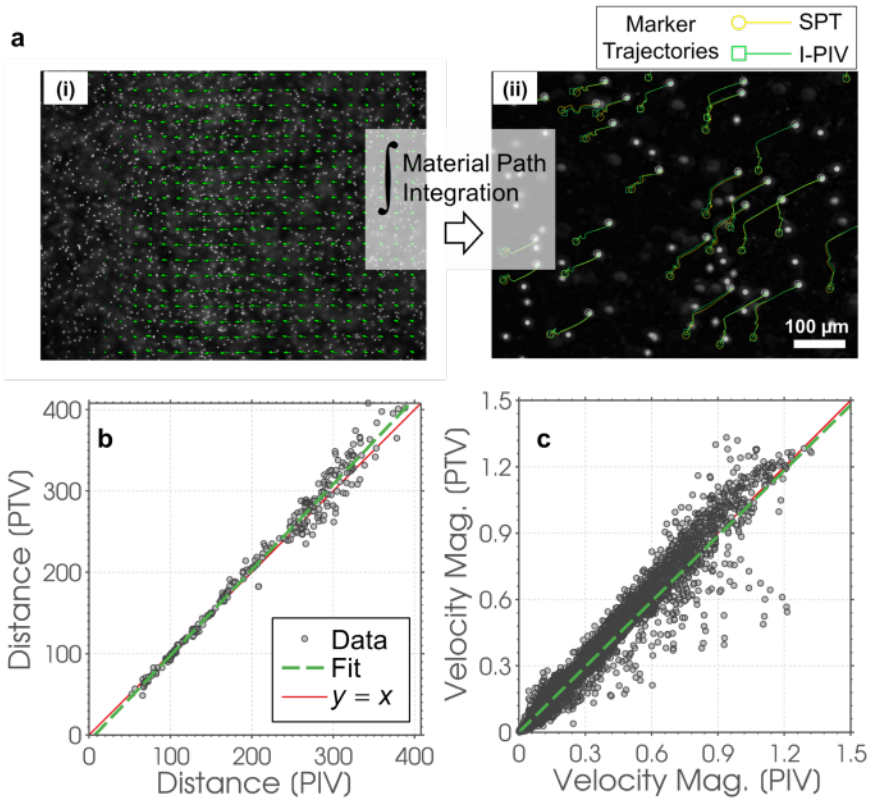

Figure S3. Measurement of matrix translocation based on tissue image deformetry. (a) (i) Fluorescence images of extracellular tracers were analyzed by particle image velocimetry (PIV) to determine the instantaneous velocity field (green arrows). (ii) The trajectories of material points on collagen matrix were calculated by material path integration of the PIV velocity field. The trajectories calculated by this incremental-PIV (I-PIV) technique were validated by comparing against tracer trajectories directly determined by single particle tracking (SPT). Comparison of (b) marker displacements and (c) velocity magnitudes obtained by I-PIV and SPT at 24 hours for 250 randomly selected tracers. y = x line indicates perfectly matching measurements.

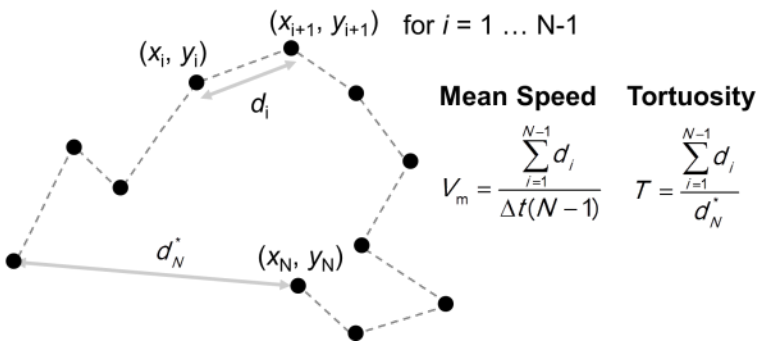

Figure S4. Schematic of a cell trajectory illustrating the calculation of mean speed and tortuosity based on distances between individual segments, d_i, and end-to-end distance d_N^*.

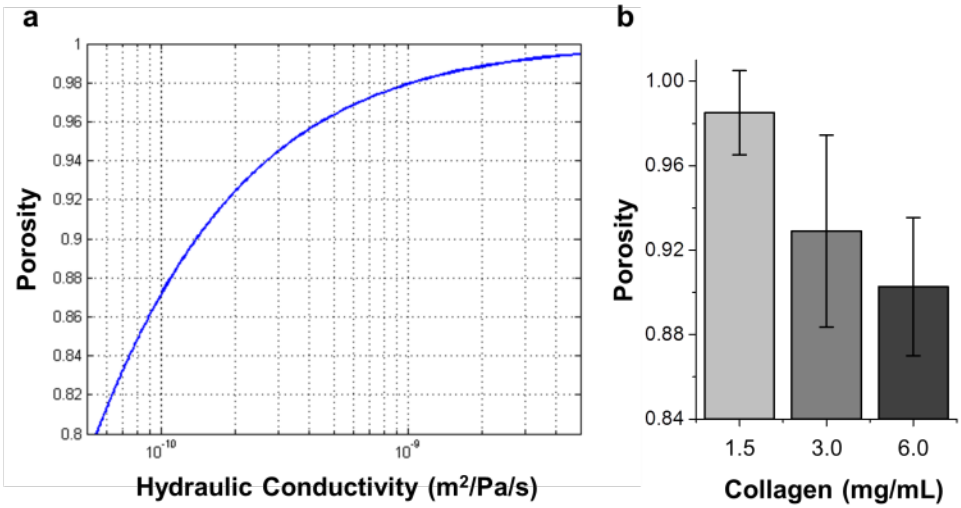

Figure S5. Estimation of porosities of collagen matrices based on hydraulic conductivity measurements. (a) Porosity as a function of hydraulic conductivity based on mathematical correlation by Jackson et al. [2] used in this study. (b) Estimated porosities of collagen matrices with different collagen concentrations.

References

[1] Armstrong CG, Lai WM, Mow VC. An analysis of the unconfined compression of articular-cartilage. Journal of Biomechanical Engineering-Transactions of the Asme. 1984;106:165-73.

[2] Jackson GW, James DF. The permeability of fibrous porous media. The Canadian Journal of Chemical Engineering. 1986;64:364-74.